Liquefaction at Oceano, California, during the 2003 San Simeon Earthquake

by Thomas L. Holzer, Thomas E. Noce, Michael J. Bennett, John C. Tinsley III, and Lewis I. Rosenberg

Abstract   The 2003 M 6.5 San Simeon, California, earthquake caused liquefaction-induced lateral spreading at Oceano at an unexpectedly large distance from the seismogenic rupture. We conclude that the liquefaction was caused by ground motion that was enhanced by both rupture directivity in the mainshock and local site amplification by unconsolidated fine-grained deposits. Liquefaction occurred in sandy artificial fill and undisturbed eolian sand and fluvial deposits. The largest and most damaging lateral spread was caused by liquefaction of artificial fill; the head of this lateral spread coincided with the boundary between the artificial fill and undisturbed eolian sand deposits. Values of the liquefaction potential index, in general, were greater than 5 at liquefaction sites, the threshold value that has been proposed for liquefaction hazard mapping. Although the mainshock ground motion at Oceano was not recorded, peak ground acceleration was estimated to range from 0.25 and 0.28g on the basis of the liquefaction potential index and aftershock recordings. The estimates fall within the range of peak ground acceleration values associated with the modified Mercalli intensity = VII reported at the U.S. Geological Survey (USGS) "Did You Feel It?" web site.

Introduction

The 22 December 2003 M 6.5 San Simeon, California, earthquake occurred on a reverse fault that previously was not recognized as active (Hardebeck *et al.*, 2004). It caused damage to buildings and lifelines in San Luis Obispo County. Although most of the damage was near the fault that produced the earthquake, significant damage occurred at Oceano, California, which was approximately 63 km from the southeastern end of the rupture surface and 80 km from the epicenter (Fig. 1). Houses, road surfaces, and underground utilities were damaged primarily by liquefaction and associated lateral spreading but also by ground shaking. Liquefaction at 63 km from a M 6.5 earthquake is unexpected and implies that special factors enhanced the earthquake ground motion at Oceano.

In this article we describe the results of subsurface exploration and analyses that were conducted to explain both the occurrence of liquefaction at 63 km from the San Simeon earthquake and the specific locations of liquefaction in Oceano. We conclude that: (1) rupture directivity and local site conditions sufficiently enhanced the ground motion at Oceano to cause liquefaction and damage, and (2) both artificial fill and undisturbed sediment liquefied, but the most damaging and largest lateral spread was caused by liquefaction of fill. The analyses rely, in part, on the liquefaction potential index (LPI), a spatial parameter for estimating liquefaction severity. We conclude that LPI predicted both levels of ground shaking and the general locations of lique-

faction. We also note the similar responses of Oceano to the 2003 San Simeon earthquake and of the Marina District in San Francisco, California, to the 1989 Loma Prieta earthquake. The similarity is a reminder of the special vulnerability to distant earthquakes of coastal communities that are underlain by both unimproved sandy artificial fills and thick, geologically young, fine-grained deposits.

The field investigation in Oceano included mapping of surface effects from the earthquake and subsurface exploration. Subsurface conditions were explored with 37 seismic cone penetration test (SCPT) soundings and 5 hollow-stem-auger borings. The auger borings were conducted at SCPT locations and were primarily used to sample intervals of interest identified during the SCPT exploration. Both standard penetration testing and sampling with Shelby tubes were conducted in the borings. Penetration data and shear-wave travel times from the 37 SCPT soundings are available at http://quake.usgs.gov/prepare/cpt/.

Earthquake Effects at Oceano

Liquefaction

Most of the damage to houses, road surfaces, and underground utilities in Oceano from the San Simeon earthquake was associated with two lateral spreads that were caused by liquefaction (Figs. 2 and 3). The larger lateral spread was
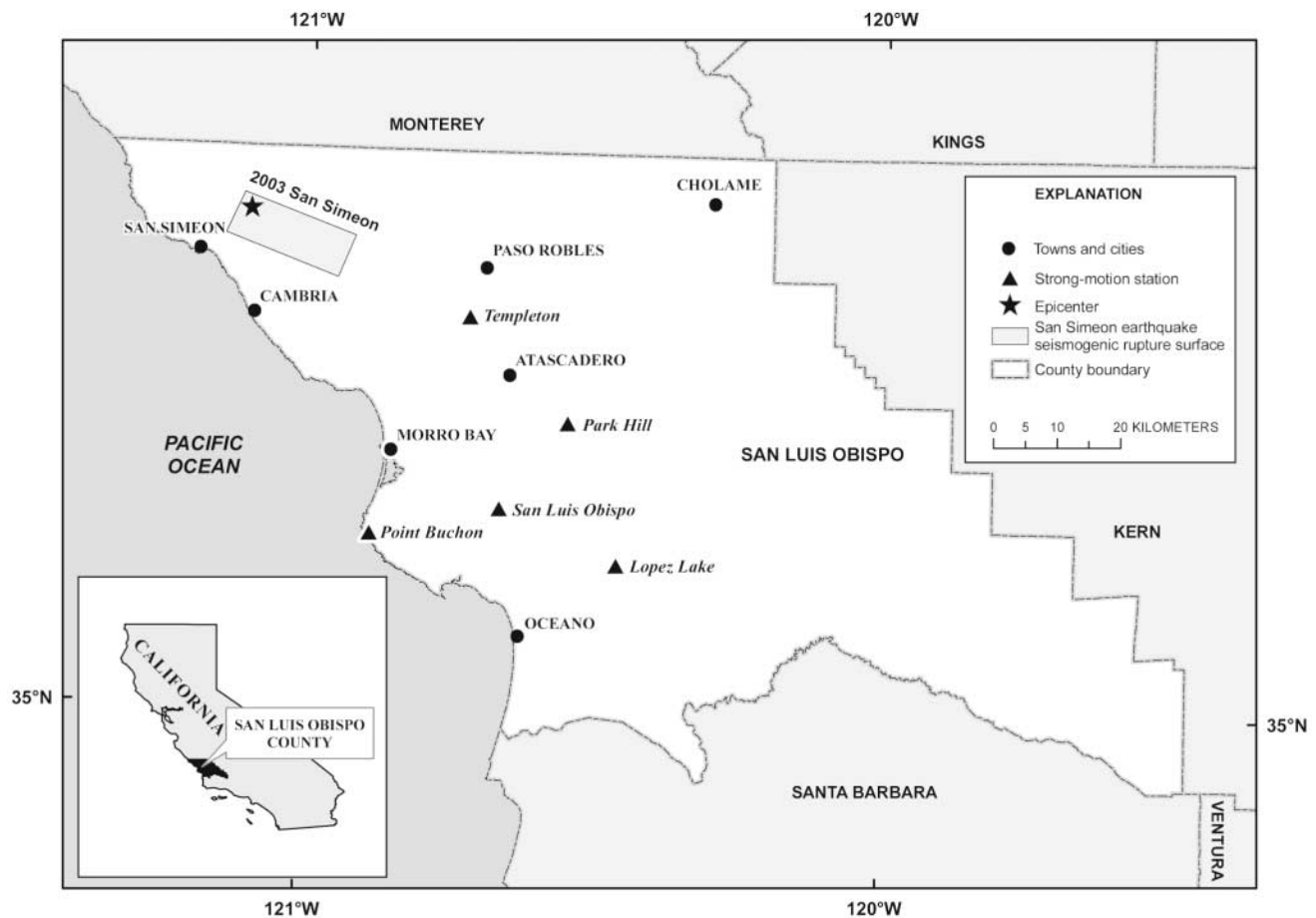
Figure 1. Map of San Luis Obispo County, California, with epicenter and rupture surface of 2003 San Simeon *M* 6.5 earthquake (Hardebeck *et al.*, 2004) and strong-motion stations along general azimuth from the 2003 earthquake to Oceano.

subparallel to Norswing Drive and will be referred to as the Norswing Drive lateral spread. The head scarp was oriented approximately north–south, and the spread slid westward. The lateral spread was 520 m wide and 75 m from head to toe where the toe was observed. The head scarp traversed obliquely across the topography, particularly on the north end. The toe was observed only at the north end of the lateral spread. Southward, the toe was either under Oceano Lagoon or a diffuse zone of compression that was difficult to identify. The other lateral spread was perpendicular to McCarthy and Juanita Avenues and will be referred to as the Juanita Avenue lateral spread. Its head scarp was oriented north–south, and the spread slid eastward. The spread was only about 75 m wide and 90 m across from head to toe. Its head scarp was defined by a broad zone of extension cracks.

Both lateral spreads formed on very gentle slopes, although the northern end of the Norswing Drive lateral spread was on a slope of about 5%. Horizontal translation was generally downslope. Cumulative horizontal displacements across ground cracks at both of the lateral spreads along their heads and toes were small (<30 cm). Discrete vertical offsets across individual ground cracks were less than 5 cm.

An eyewitness report to the U.S. Geological Survey (USGS) "Did You Feel It?" web site described the dynamics of the Norswing Drive lateral spread. The eyewitness, who was looking out of a window at the house next door that was damaged by the lateral spread (Fig. 3), reported that the crack in the masonry wall opened during the strong ground shaking. Because the crack was on the head scarp of the lateral spread, its early appearance suggests that the spread may have been an inertial rather than a flow failure. If the failure had been a flow mechanism, we would have expected the crack to form slowly and deformation to continue after shaking stopped, at least until excess pore pressures dissipated.

Several smaller ground failures and lateral spreads also were observed in Oceano (Fig. 2). The most significant of these was a bearing-capacity failure that damaged the southern levee of Arroyo Grande Creek (at sounding 35). The failure was associated with liquefaction; sand boils erupted over a large area in a ranch pasture adjacent to and south of the levee. An eyewitness of the liquefaction in the pasture reported that muddy water began erupting from the ground and along cracks about 10–15 mins after the shaking stopped
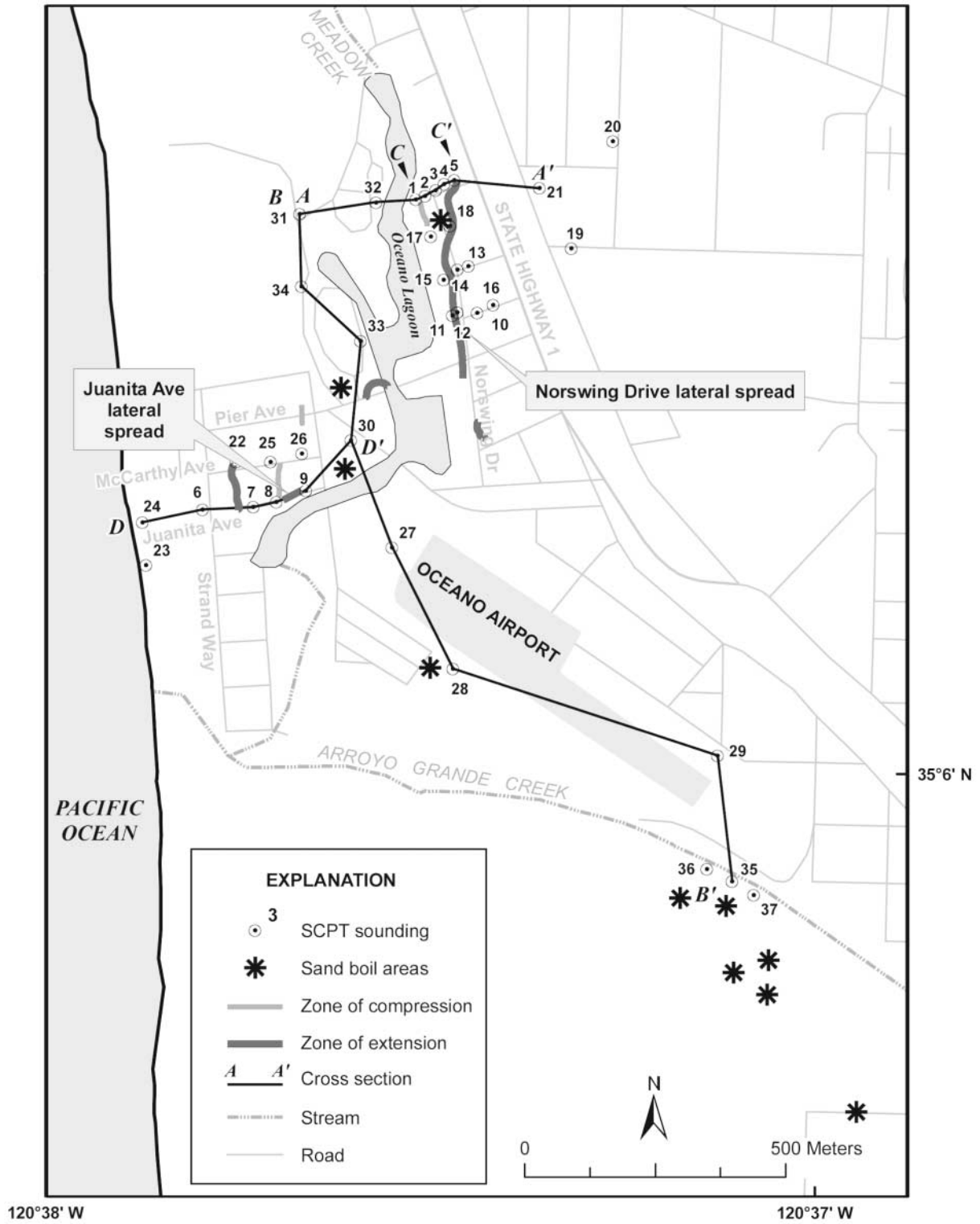
Figure 2.   Map of Oceano, California, with locations of sand boils and lateral spreads caused by 2003 San Simeon earthquake, SCPT soundings, and cross sections.

Figure 3. Damaged house at 1157 Norswing Drive, Oceano, California. Masonry wall and foundation cracked along head scarp of lateral spread during earthquake. House was subsequently razed. Photograph by Thomas L. Holzer.

and that large volumes of water continued to discharge for as long as about 30 min after the earthquake (Holzer *et al.*, 2004).

Liquefaction is unexpected at 63 km from a *M* 6.5 earthquake. This is illustrated in Figure 4, which compares the location of Oceano with the maximum distance to liquefaction predicted by Ambraseys (1988). Distance is measured from the closest point on the seismic source zone; the earthquake magnitude is moment magnitude. Ambraseys' predicted maximum distances are based on 102 case histories. For the *M* 6.5 San Simeon earthquake, liquefaction should not be observed more than approximately 40 km from the seismic source zone.

Shaking

Although permanent ground deformation caused most of the damage in Oceano, shaking also directly contributed to damage. This damage consisted of unattached objects falling during the mainshock, cracking in walls of single- and two-story wood-frame structures, and toppled chimneys.

Mainshock ground motion was not instrumentally re-

corded at Oceano, but strong ground shaking was reported by eyewitnesses to the USGS at its "Did You Feel It?" web site (http://pasadena.wr.usgs.gov/shake/ca/STORE/X40148755/ciim_display.html). These reports are compiled by zip code. The 19 responses from the Oceano zip code (93445) yield a median modified Mercalli intensity (MMI) of VII, which Wald *et al.* (1999) associate with peak ground accelerations (PGA) that range from 0.18 to 0.32*g*. The accounts also indicate that shaking was higher at Oceano than in surrounding communities, where median intensities ranged from MMI V to VI, which correspond to PGAs that range from 0.04 to 0.18*g*.

The San Simeon earthquake was caused by a unilateral fault rupture to the southeast (Hardebeck *et al.*, 2004). Boatwright and Seekins (2004) report that the "unilateral rupture is clearly expressed in the peak ground acceleration (PGA) . . . recorded at stations as far as 300 km to the northwest and southeast of the earthquake." They observed that PGAs recorded southeast of the mainshock were almost three times higher than PGAs recorded to the northwest. This effect on ground motion, known as rupture directivity, can be seen in mainshock PGAs recorded at the five strong-motion stations that are located between the 2003 San Simeon earthquake rupture surface and Oceano, the approximate direction of fault rupture (see Fig. 1 for locations). The PGA recorded at four of these five stations is a factor of 2 larger than median PGA values for reverse-fault earthquakes estimated by Boore *et al.* (1997) for soft-rock site conditions (V_{S30} = 620 m/sec) (Fig. 5). Although the comparison in Figure 5 is to a soft rock site condition, the higher observed PGAs at the five stations do not appear to be caused by local site effects. Observed PGAs also are larger than values predicted for a V_{S30} = 360 m/sec site condition, the lower velocity boundary for National Earthquake Hazards Reduction Program (NEHRP) site class C (BSSC, 2001) (Fig. 5). NEHRP site classifications of the five stations range from B to C according to mapping by Wills *et al.* (2000). Rupture directivity, however, accounts for only part of the higher ground motion at Oceano. The range of PGA at Oceano inferred from "Did You Feel It?" is higher than the PGA inferred from the trend of strong-motion stations affected by directivity (Fig. 5). Thus, additional factors appear to have enhanced the shaking at Oceano. These factors will be discussed in the section Mainshock PGA at Oceano after the engineering geology of Oceano and other PGA estimates that were inferred from aftershocks and liquefaction are described.

Engineering Geology

Oceano is directly underlain by an approximately 240-m-thick sequence of gently westward-dipping unconsolidated sediment that has been the subject of investigations prompted by saltwater intrusion into the coastal aquifer beneath Oceano and the surrounding area (Weber and Hanamura, 1970). The uppermost sediment (<30 m) consists of a complexly interbedded sequence of unconsolidated dune
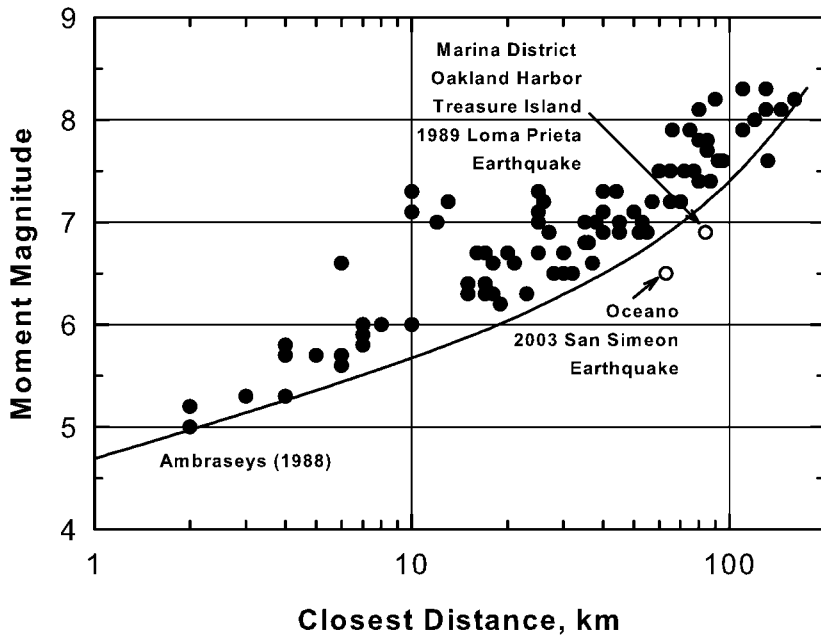
Figure 4.   Predicted maximum distance to liquefaction versus moment magnitude (Ambraseys, 1988) and observed distances for Oceano in 2003 and liquefaction sites along the margin of San Francisco Bay during the 1989 Loma Prieta (*M* 6.9) earthquake. Filled circles are case histories compiled by Ambraseys (1988).
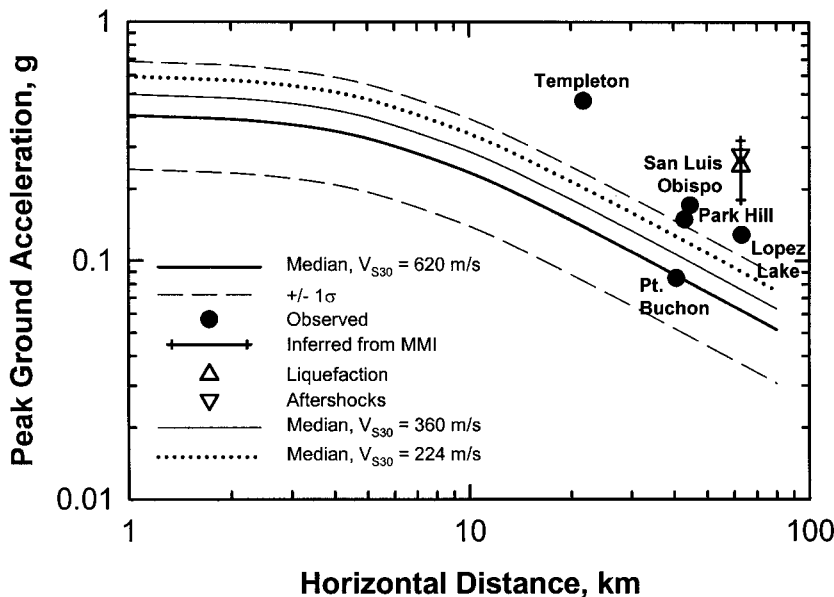
Figure 5.   PGA recorded at strong-motion stations along general azimuth from the 2003 San Simeon earthquake to Oceano compared with the estimated median ($\pm 1\sigma$) PGA at soft-rock sites ($V_{S30} = 620$ m/sec) and median PGAs at site conditions for dense soil ($V_{S30} = 360$ m/sec) and at Oceano ($V_{S30} = 224$ m/sec) for a *M* 6.5 reverse-fault earthquake (Boore *et al.*, 1997). Range of PGA inferred from MMI at Oceano as reported to USGS "Did you feel it?" web site and PGA inferred from liquefaction and aftershocks are also shown.

sand, shallow marine and estuarine deposits, and fluvial sediments of Meadow and Arroyo Grande Creeks. These sediments, which are locally buried by artificial fill, overlie beds that are equivalent to the Lower Pleistocene Paso Robles Formation and 140 m of Upper Pliocene Careaga Sand, which is of primarily marine origin (Weber and Hanamura, 1970). These unconsolidated sediments rest on Lower to Upper Pliocene Pismo Sandstone.

Predevelopment surficial geologic conditions in Oceano can be inferred from the 1873–1874 U.S. Coast Survey T-sheet 1393 (Fig. 6). The map portrays areas of both active and inactive sand dunes, marsh and tidal estuarine deposi-

tion, floodplains of Arroyo Grande and Meadow Creeks, and beach deposition. The T-sheet delineates an extensive marsh along Meadow and Arroyo Grande Creeks, most of which was filled in by leveling dunes in March 1927 (J. D. McGregor, 1927, unpublished subdivision map, San Luis Obispo County Assessor's Office). The modern lagoon on Meadow Creek—Oceano Lagoon—is the only remaining trace. The uppermost sediments at Oceano consist of a 5- to 8-m-thick complex of eolian (windblown), fluvial, tidal, marsh, and artificial fill deposits (Figs. 7a and 8a). Although each deposit has a distinctive cone penetration test (CPT) profile signature, distinguishing between the fill and eolian
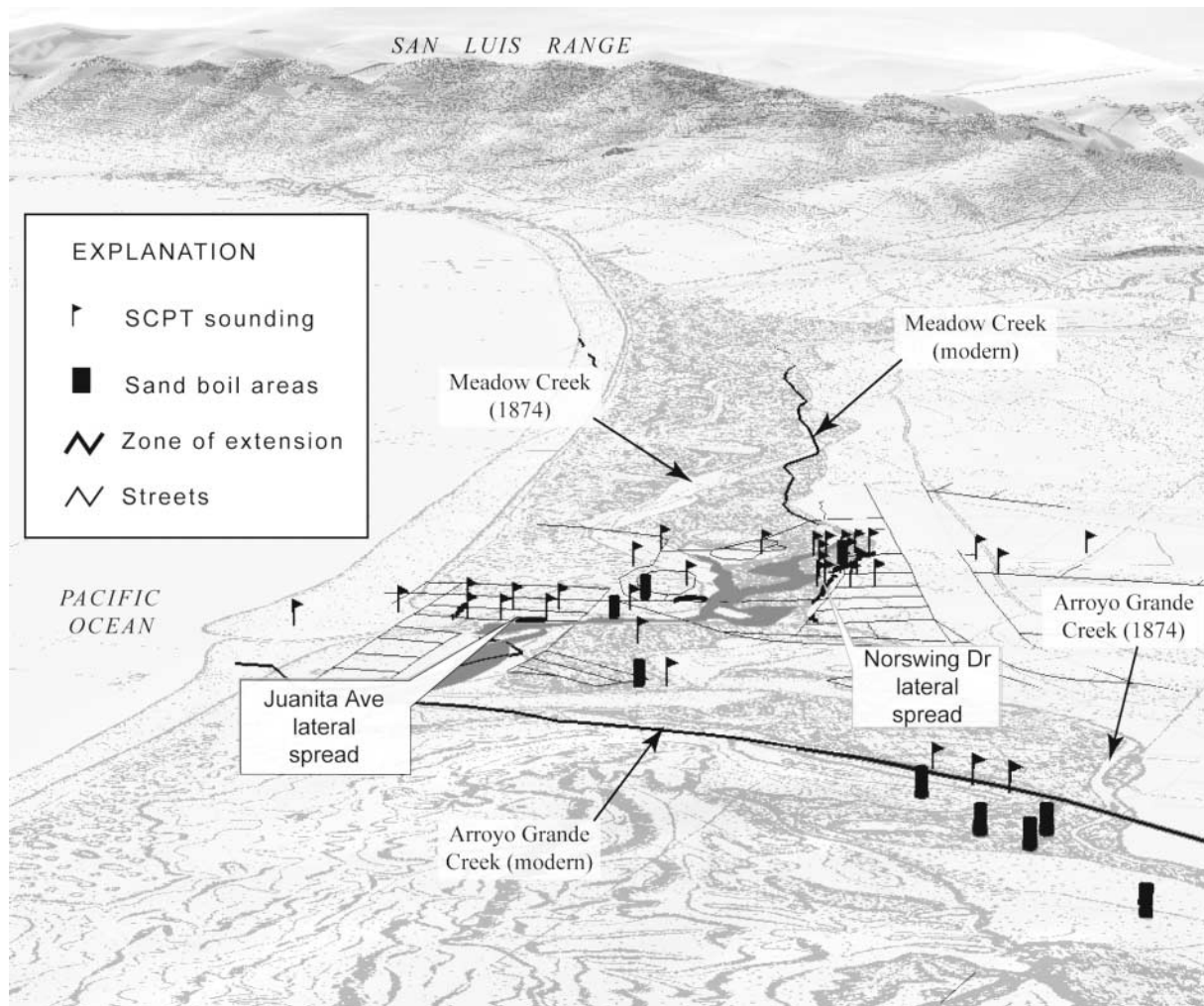
Figure 6. Northward oblique view of 1873–1874 U.S. Coast Survey T-sheet 1393 of Oceano area showing predevelopment marsh and sand dunes superimposed on a digital elevation model. Modern street grid, Oceano Lagoon, SCPT soundings, and 2003 liquefaction are superimposed. Note head scarp of Norswing Drive lateral spread coincides with boundary between 1874 marsh and sand dunes.

sand where they were in direct contact was difficult. To identify fill, we relied on its slightly lower shear-wave velocity and its very low sleeve friction. This shallow sedimentary complex rests on a laterally continuous 5- to 9-m-thick sand layer, which we interpret from core samples to be primarily a beach and estuarine sand deposit. The beach and estuarine sand deposit in turn rests on an estuarine-bedded clayey silt deposit of unknown thickness that contains discontinuous sand lenses.

Geotechnical properties of four of the geologic units are summarized in Table 1. Properties are based on samples that were retrieved from five auger borings. Soil texture of the eolian deposits and artificial fill is dominated by fine, well-sorted sand (SP) and sand with silt (SP-SM) as classified with the Unified Soil Classification System (USCS) ASTM D2487. The texture of the artificial fill and eolian sand are similar. Their median grain sizes (D_{50}), fines contents, and

sorting ($D_{60}/D_{10} = 1.7$) are comparable. This is not surprising because the fill was placed by reworking and tipping undisturbed eolian sand into the former marsh. The underlying estuarine and beach sand deposit is slightly coarser ($D_{50} = 0.197$ mm) and more poorly sorted ($D_{60}/D_{10} = 2.9$) in a geologic sense, but it also is fairly clean, averaging only 7% fines. The low fines content of these three units indicates that the fines correction in the liquefaction analyses should be minimal. The estuarine silty clay was the finest-grained sediment sampled in Oceano. Its D_{50} is 0.004 mm and clay content (<0.005 mm) is 55%. The sediment is fat clay (CH) based on a liquid limit of 73 and a plasticity index (PI) of 44. The sand layers that are interbedded in the silty clay are poorly sorted, fine-grained, silty clayey sand (SC-SM). Their fines and clay contents, respectively, are 34% and 16%. The liquid limit is 26 and the PI is 6.

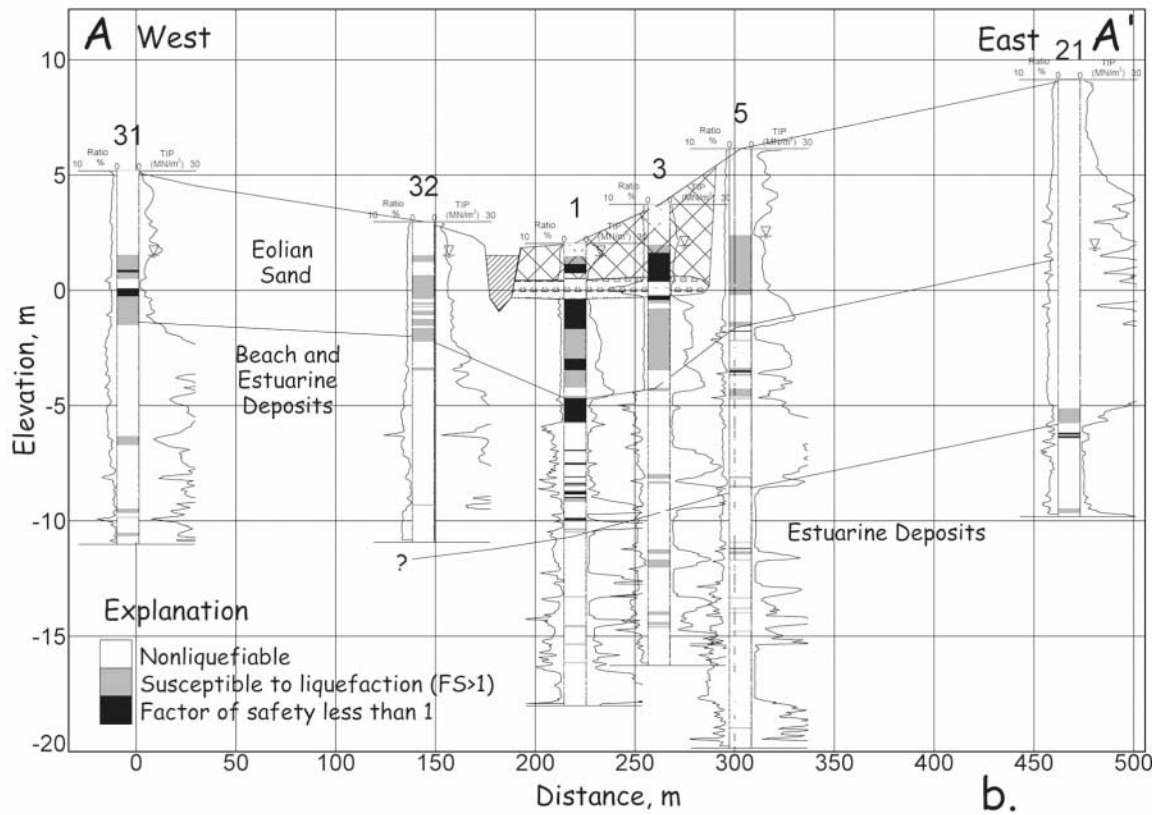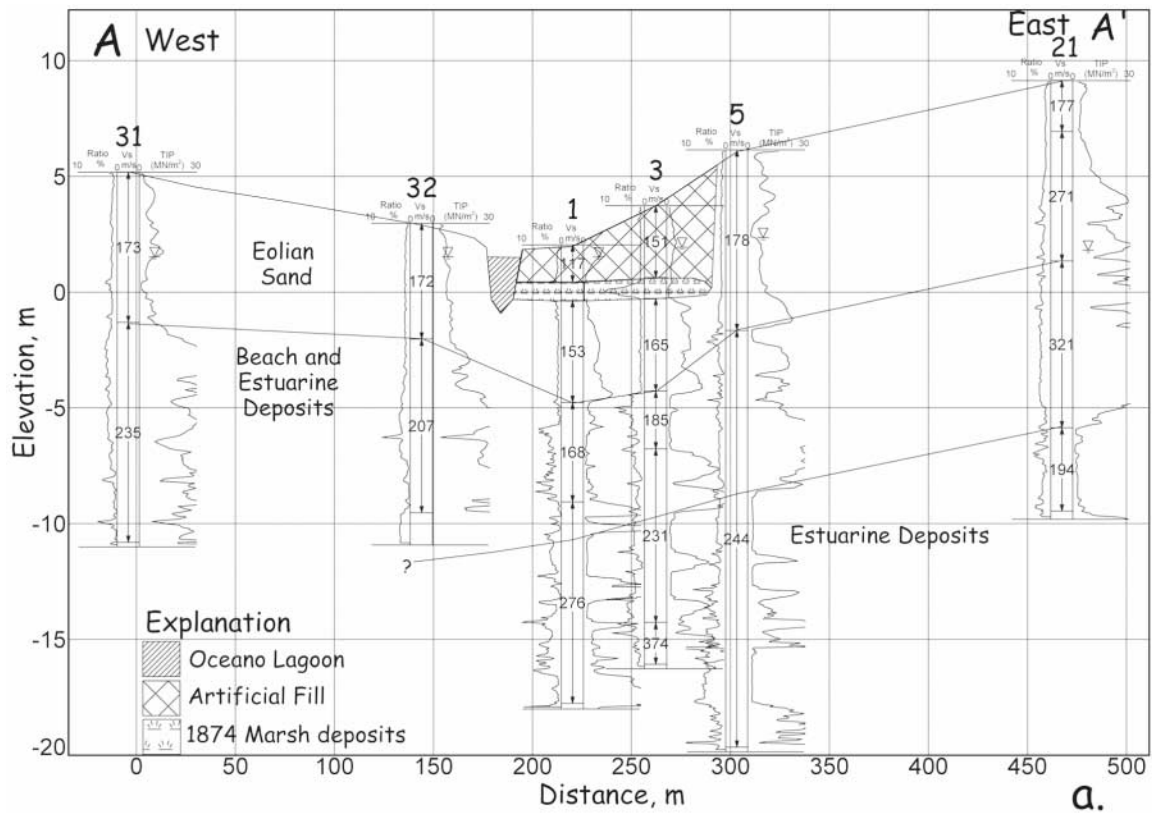Depth to the water table at Oceano varies with the to-

Figure 7. West–east cross section (AA′) at Oceano showing (a) geologic units and (b) factors of safety based on SCPT soundings for San Simeon earthquake (PGA = 0.25*g*). See Figure 2 for location. Cross section in (a) includes CPT tip resistance and friction ratio, shear-wave velocity (m/sec) of SCPT soundings, and geologic units. Water table at sounding is shown by inverted triangle.

Figure 8.   North–south cross section (BB′) at Oceano showing (a) geologic units and (b) factors of safety based on SCPT soundings for San Simeon earthquake (PGA = 0.25*g*). See Figure 2 for location. Cross section in (a) includes CPT tip resistance and friction ratio, shear-wave velocity (m/sec) of SCPT soundings, and geologic units. Water table at sounding is shown by inverted triangle.
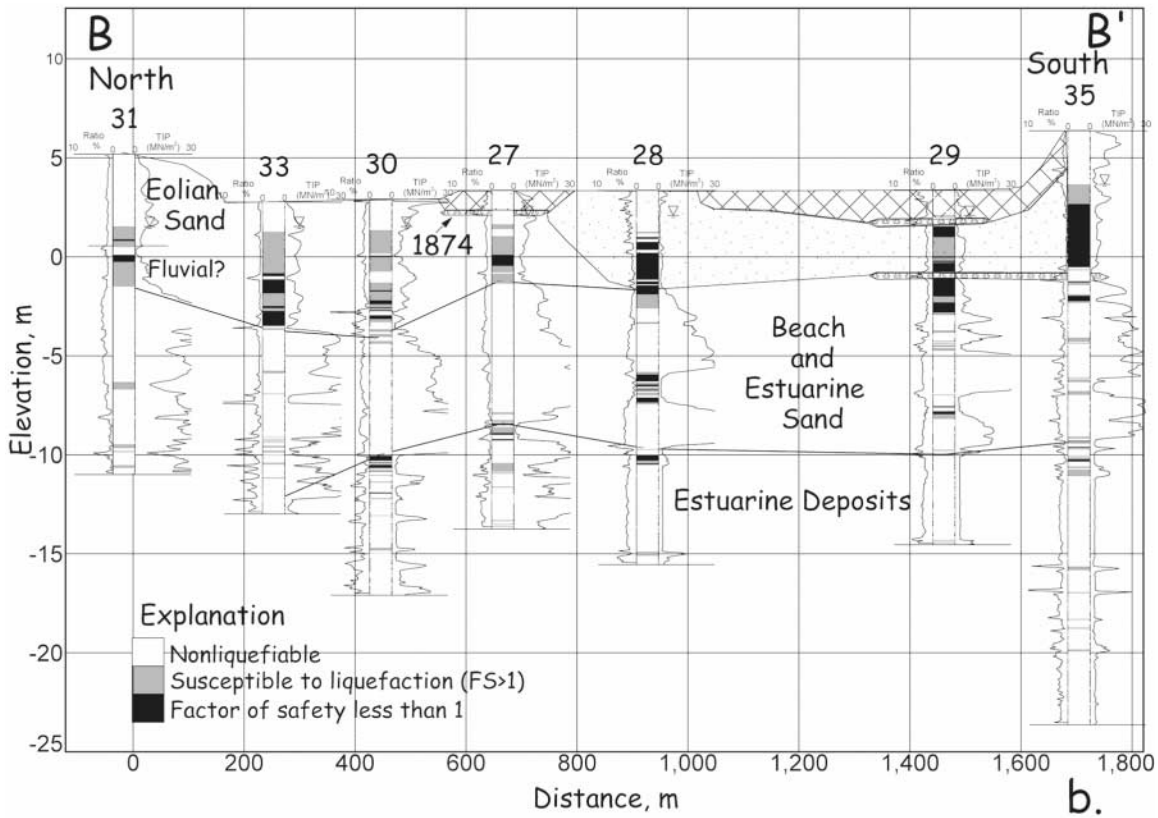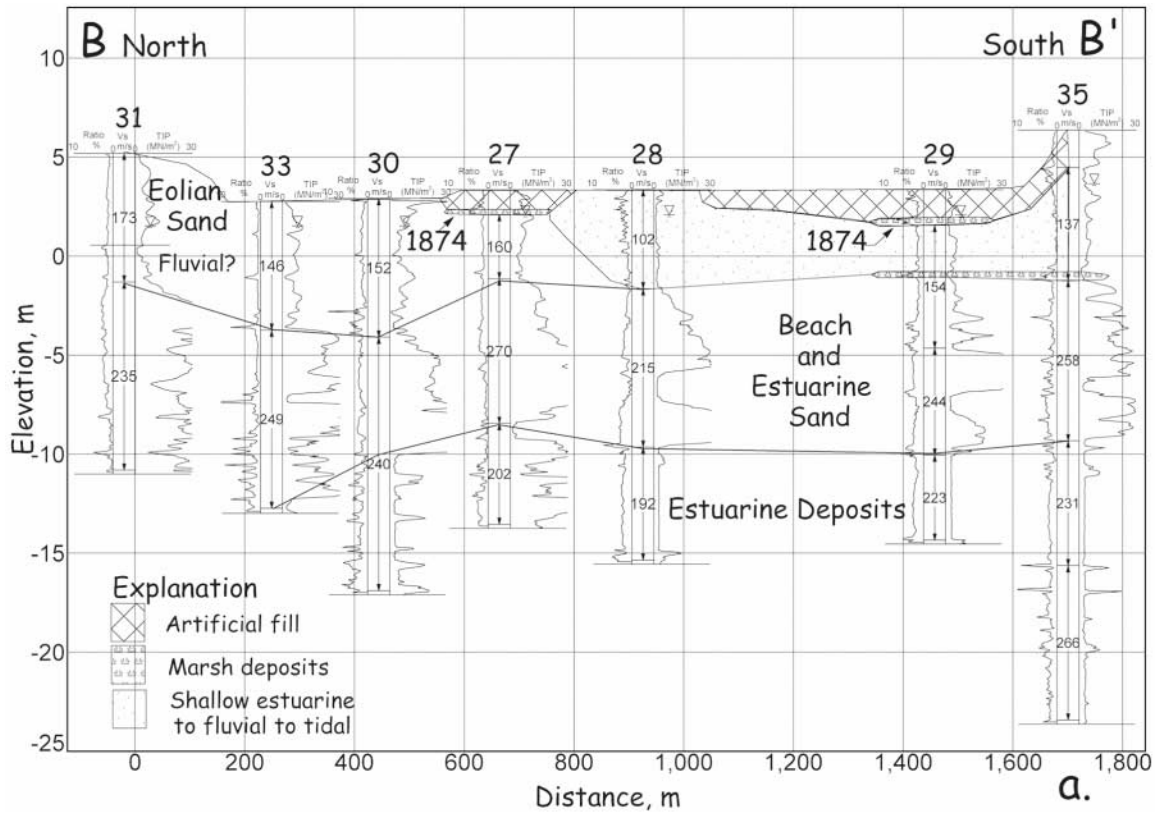
pography of the sand dunes. In general, depths are proportional to topographic elevation and range from 0.52 to 11.6 m. Most of the liquefaction, however, occurred in low-lying areas where depths to water were generally around 1 m. Water table information is available in Holzer *et al.* (2004).

Mainshock PGA at Oceano

Independent estimates of the mainshock PGA at Oceano were inferred from aftershock recordings and the occurrence of liquefaction. The estimates are compared in Figure 5 with (1) the range of PGA inferred from MMI as reported at the "Did You Feel It?" web site, and (2) PGA predicted for reverse faulting by Boore *et al.* (1997) for a soft-rock site ($V_{S30} = 620$ m/sec), dense-soil site ($V_{S30} = 360$ m/sec), and the measured V_{S30} at Oceano (224 m/sec).

The method for estimating PGA from aftershocks is described by Di Alessandro and Boatwright (2006) and is briefly summarized here. They used the generalized method of spectral ratios developed by Boatwright *et al.* (1991) to estimate the mainshock spectrum from aftershocks that were recorded by the USGS with a portable seismograph deployed on the Norswing Drive lateral spread. In this method, the mainshock Fourier amplitude spectra recorded at nearby strong-motion stations is multiplied by the spectral ratio of the aftershocks recorded at Oceano and the same strong-motion stations. To estimate the mainshock PGA, they first test a set of aftershocks as Green's functions by comparing simulated and recorded acceleration amplitude for the mainshock at the strong-motion stations. The aftershock accelerograms are then convolved with a stochastic operator to simulate the phase and duration of the mainshock accelerograms. Di Alessandro and Boatwright (2006) estimate that the mainshock PGA at Oceano was $0.28 \pm 0.04g$, where the variability results from different realizations of the stochastic operator. The method of spectral ratios assumes that the soil responded linearly during the mainshock. It may overestimate the acceleration for soft soil sites because soil at these sites can behave nonlinearly if shaking is strong. Thus, $0.28g$ is interpreted as an upper bound for PGA.

PGA at Oceano also was estimated with the LPI at the

lateral spreads. LPI is a depth-weighted integration of one minus the liquefaction factors of safety at a specific location. Factors of safety were computed here from soundings. LPI is described in greater detail in Appendix A. The approach to estimate PGA with LPI relies on the calibration by Toprak and Holzer (2003) that an LPI ≥ 5 predicts surface mani-
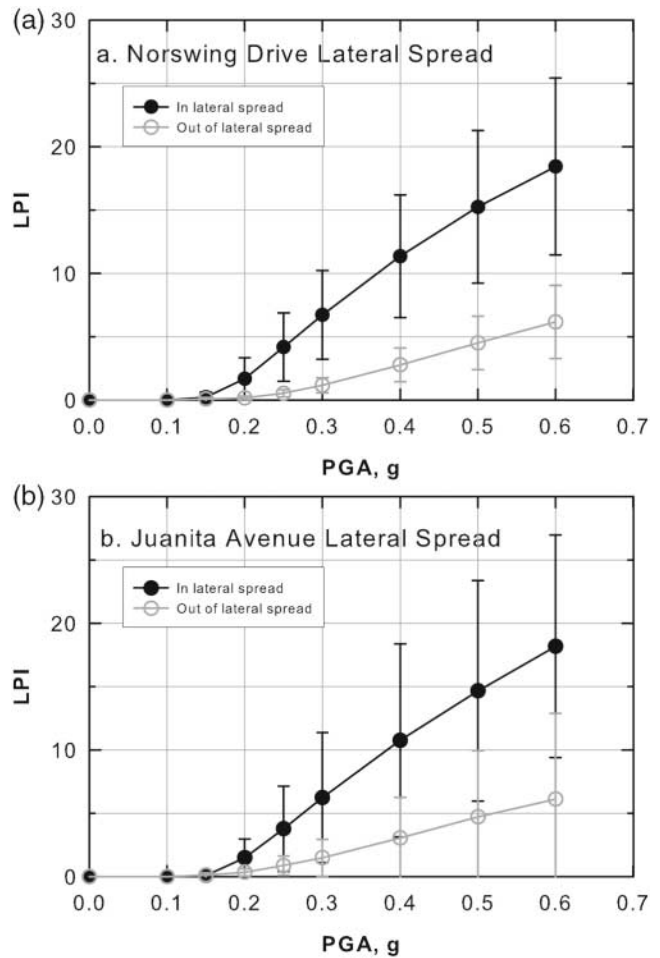

Figure 9.   Median LPI ($\pm 1\sigma$) for soundings in and out of (a) Norswing Drive and (b) Juanita Avenue lateral spreads as a function of PGA. LPI computed for *M* 6.5 earthquake.

Table 1
Average Soil Properties of Samples from USGS Borings at Oceano

Unit	Thickness (m)	D_{50} (mm)	Fines (<75 μm) %	Clay (<5 μm) %	Water Content %	Atterburg Limit, % LL	Atterburg Limit, % PL	V_s (m/sec)	q_{c1N} (MN/m²)	USCS
Artificial fill	2.4	0.152	5.5					139	9.5	SP-SM, SM
Eolian sand	5.2	0.157	7.1		14			186	13.3	SP-SM, SM
Beach and estuarine	7.5	0.197	7.0					247	24.8	SP, SP-SM
Estuarine										
Fine-grained	>4.3	0.004	94.0	55	42	73	29	225	1.8	CH
Coarse-grained	>3.5	0.140	34.0	16		26	20	267	12.5	SC-SM

q_{c1N} = normalized CPT tip resistance.

festations of liquefaction. Results are shown in Figure 9. To create Figure 9, LPI values were computed for different values of PGA for an *M* 6.5 earthquake with each SCPT sounding at the two major lateral spreads. Values were then grouped according to whether the sounding was either in or out of the lateral spread; mean LPI values were then computed for each group. Figure 9 indicates that a PGA of at least 0.25*g* (0.26*g* at Norswing Drive and 0.27*g* at Juanita Avenue) is required to produce a mean value of LPI equal to 5. Based on the variability of LPI as shown by $\pm 1\sigma$ in Figure 9, estimates of PGA range from 0.22 to 0.36*g* at both Norswing Drive and Juanita Avenue. Because LPI values are generally greater than 5 in areas of cracking and lateral spreading (see Toprak and Holzer, 2003), the PGA required to produce LPI = 5 is the minimum level of shaking that Oceano is likely to have experienced. Thus, 0.25*g* is a lower bound for PGA.

All three estimates of the mainshock PGA at Oceano are greater than the value that is inferred from PGAs recorded at the five strong-motion stations (Fig. 5). This suggests that rupture directivity does not solely explain the elevated shaking levels at Oceano and that ground shaking was locally amplified relative to the average site condition at the five strong-motion stations. We suspect that soil conditions at Oceano are the primary cause of the amplification, although focusing and wave trapping by two- and three-dimensional geologic structure may also have contributed. First, the average V_{S30} ($\pm 1\sigma$) at Oceano measured in the 37 SCPT soundings is 224 $\pm$ 21 m/sec (Holzer *et al.*, 2004), which corresponds to NEHRP site class D (180 m/sec $< V_{S30} <$ 360 m/sec). Site class D has the second highest potential for amplification of classes in the NEHRP classification (BSSC [Building Seismic Safety Council], 2001). Potential for amplification is also indicated by the high plasticity index (PI = 44) of the estuarine silty clay beneath Oceano (Vucetic and Dobry, 1991). Second, Di Alessandro and Boatwright (2006) estimate that the mainshock spectrum at Oceano exceeds the spectrum at nearby stations (San Luis Obispo and Park Hill) in the frequency band from 0.2 to 3.0 Hz. This relative amplification is consistent with the 240-m-thick sequence of unconsolidated sediment beneath Oceano. In general, the thicker the sediment, the broader range of periods that are amplified. The PGA of only 0.09*g* predicted at Oceano by Boore *et al.* (1997) with the measured V_{S30}, 224 m/sec, supports the suggestion that either or both deep ($>$30 m) sediments and basin structure contributed to the amplification of PGA (Fig. 5).

Liquefaction and Lateral Spreading

Most of the damaging liquefaction at Oceano was in artificial fill, although some liquefaction was in undisturbed eolian and fluvial deposits. This is indicated by liquefaction factors of safety (FS) that were computed with the simplified procedure (Youd *et al.*, 2001) (Figs. 7b and 8b). Each FS is the ratio of the capacity of the soils to resist liquefaction, which is computed from the SCPT penetration resistance, to the seismic demand imposed by an *M* 6.5 earthquake and a PGA = 0.25*g* (see Appendix A). Liquefaction is indicated where FS < 1. In Figure 7b, although both shallow eolian sand and artificial fill are predicted to be susceptible to liquefaction, the artificial fill is characterized by lower CPT tip resistances and FS than is the eolian sand. In Figures 7b and 8b, liquefaction of undisturbed eolian sand occurs in thin discontinuous pockets.

Significant liquefaction is predicted in the complexly interbedded sequence of fluvial, tidal, and eolian deposits south of sounding 27 (Fig. 8b). Textural properties of sand boils and core samples indicate that this liquefaction is primarily in the fluvial sediments. The evidence for this is strongest at sounding 28 where sediment observed in core samples in the upper 5 m from an adjacent boring was cross bedded, was of dark-gray color, and contained reworked shell fragments. The fluvial nature of the layer with FS < 1 from 4 to 7 m at sounding 35, which is at the bearing-capacity failure of the levee along Arroyo Grande Creek, is more speculative because the site was not sampled. Two lines of evidence suggest fluvial deposits liquefied at sounding 35. First, profiles of tip resistance and friction ratio in the interval with FS < 1 are similar to the SCPT profile in sounding 28 where sampling indicated fluvial deposits. And second, sand boils in the nearby pasture area were inferred on the basis of their dark color, sorting, and clast lithology to be vented from beds of fluvial origin.

Larger-scale cross sections across the Norswing Drive and Juanita Avenue lateral spreads show the liquefied intervals in greater detail and provide insight into the lateral spreads (Figs. 10b and 11b). The cross section of the Norswing Drive lateral spread (Fig. 10b) is an expansion of the cross section in Figure 7b between soundings 1 and 5. The laterally continuous 1- to 1.5-m-thick interval at the base of the artificial fill in which FS < 1 indicates where the lateral spread was mobilized by the liquefaction. Although portions of the undisturbed eolian sand beneath the 1874 marsh layer may have liquefied, these intervals are not laterally continuous and, thus, are unlikely to have contributed to the spreading. Intervals with FS < 1 in the larger-scale cross section across the Juanita Avenue lateral spread (Fig. 11b) indicate that both artificial fill and eolian sediment liquefied. In the central part of the lateral spread at sounding 9, liquefaction is limited to the artificial fill. Artificial fill, however, was not identified in sounding 7 on the west side of the lateral spread, and the liquefaction is inferred to have been in a 2.5-m-thick interval of undisturbed eolian sand.

The larger-scale cross sections (Figs. 10 and 11b) and T-sheet (Fig. 6) document the geologic conditions that controlled the boundaries of the two major lateral spreads. The controlling conditions are clearest for the Norswing Drive lateral spread where both the cross section and T-sheet indicate the head scarp is coincident with the contact between the artificial fill and the undisturbed eolian sand (Fig. 10b). This is also the eastern boundary of the 1874 marsh (Fig. 6).
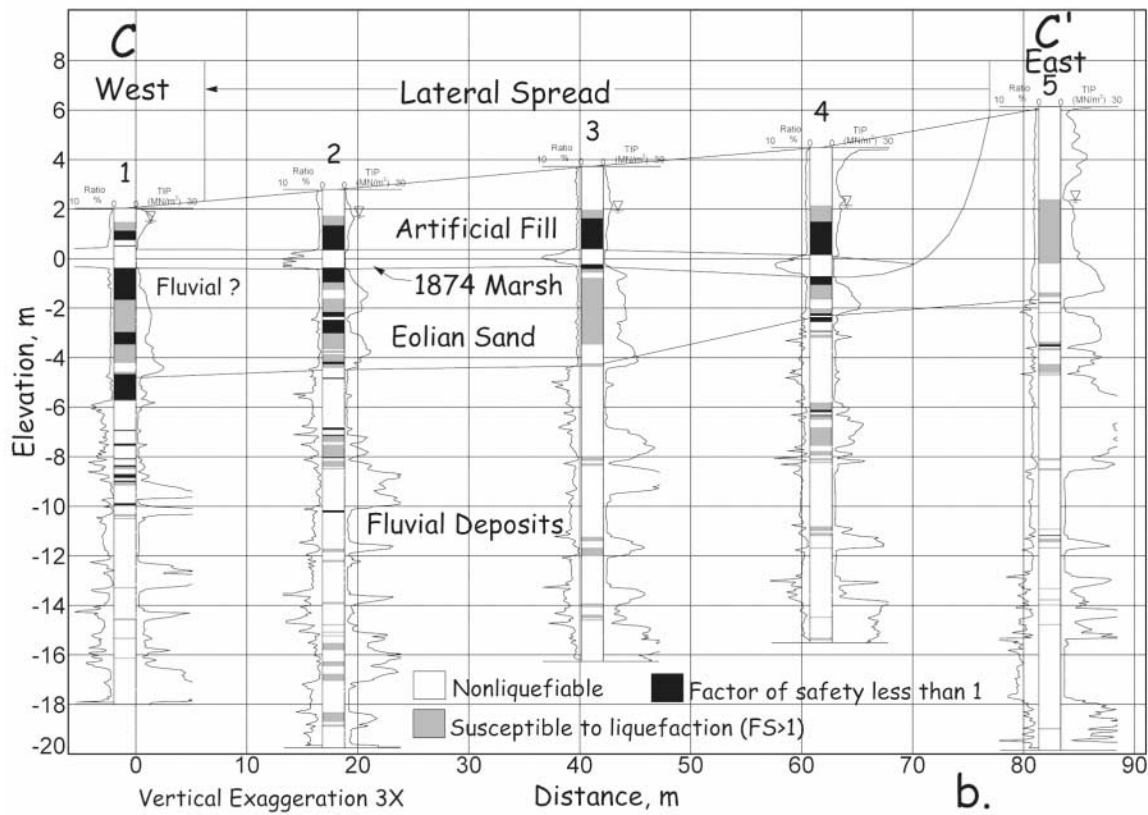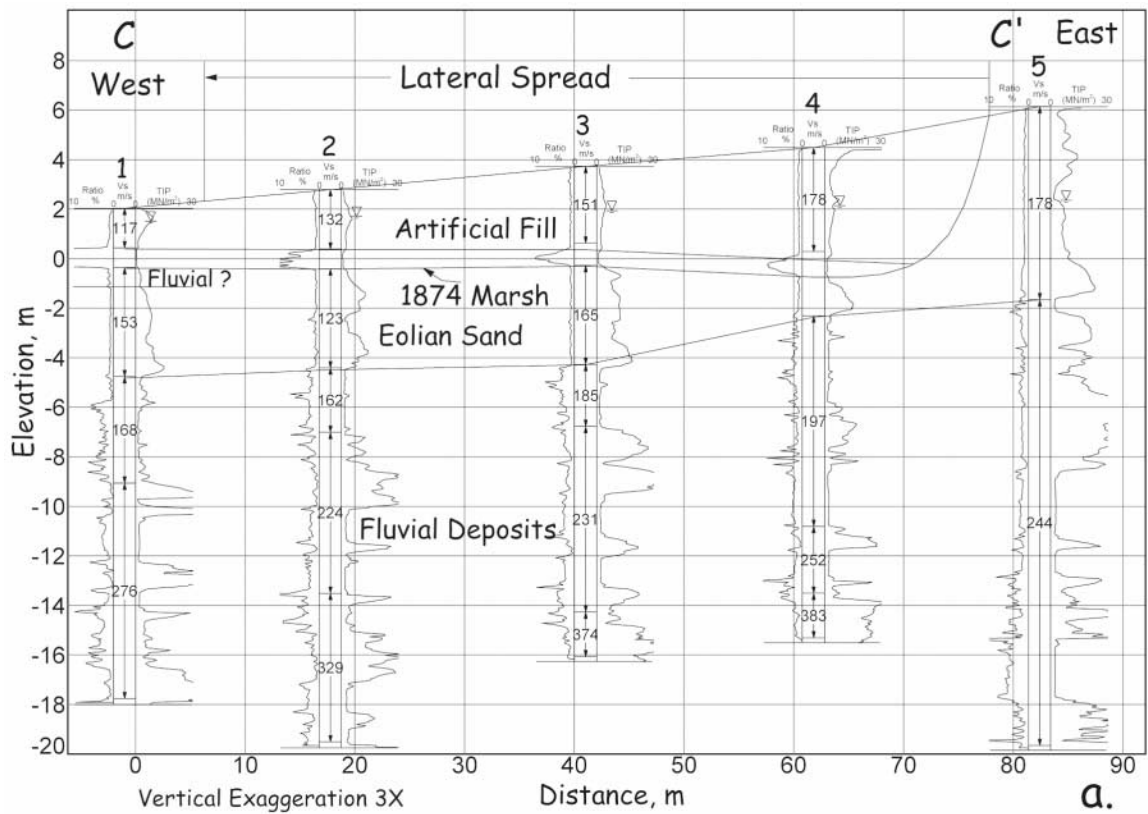
Figure 10.   West–east cross section (CC′) at Norswing Drive lateral spread showing (a) geologic units and (b) factors of safety based on SCPT soundings for San Simeon earthquake (PGA = 0.25g). See Figure 2 for location. Cross section in (a) includes CPT tip resistance and friction ratio, shear-wave velocity (m/sec) of SCPT soundings, and geologic units. Water table at sounding is shown by inverted triangle.
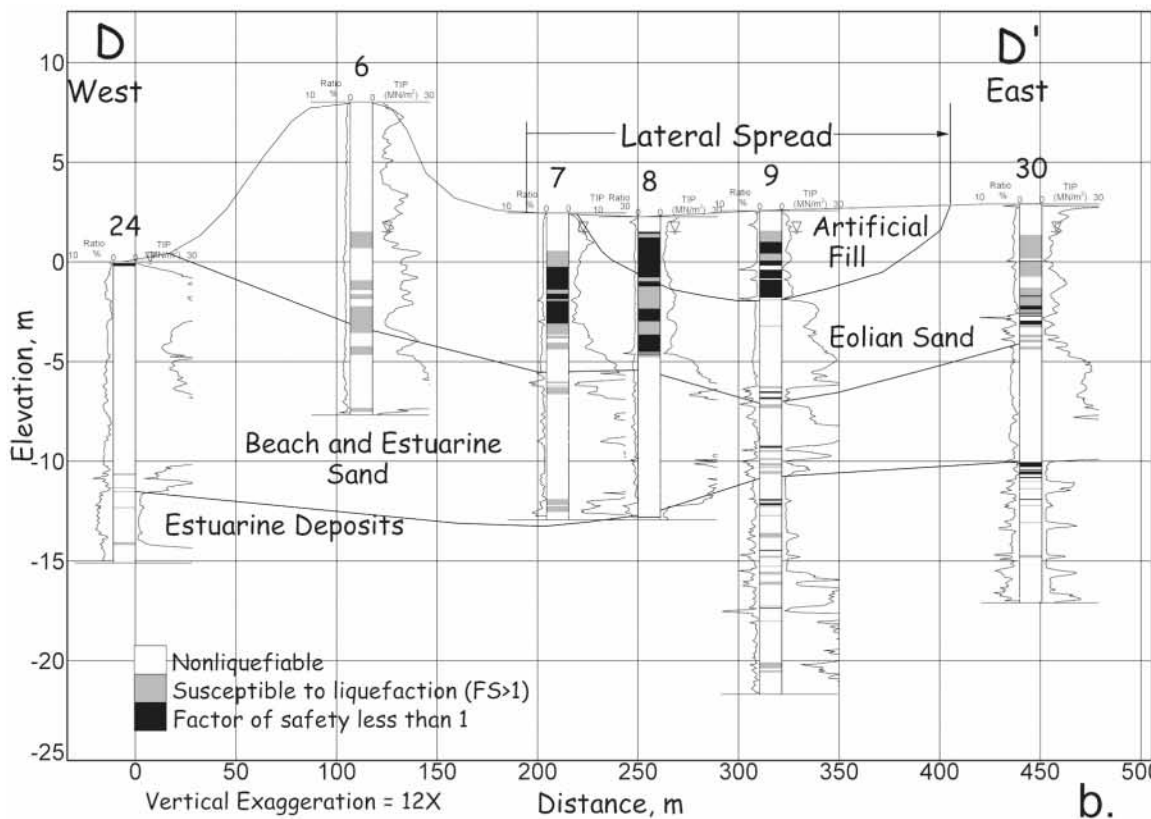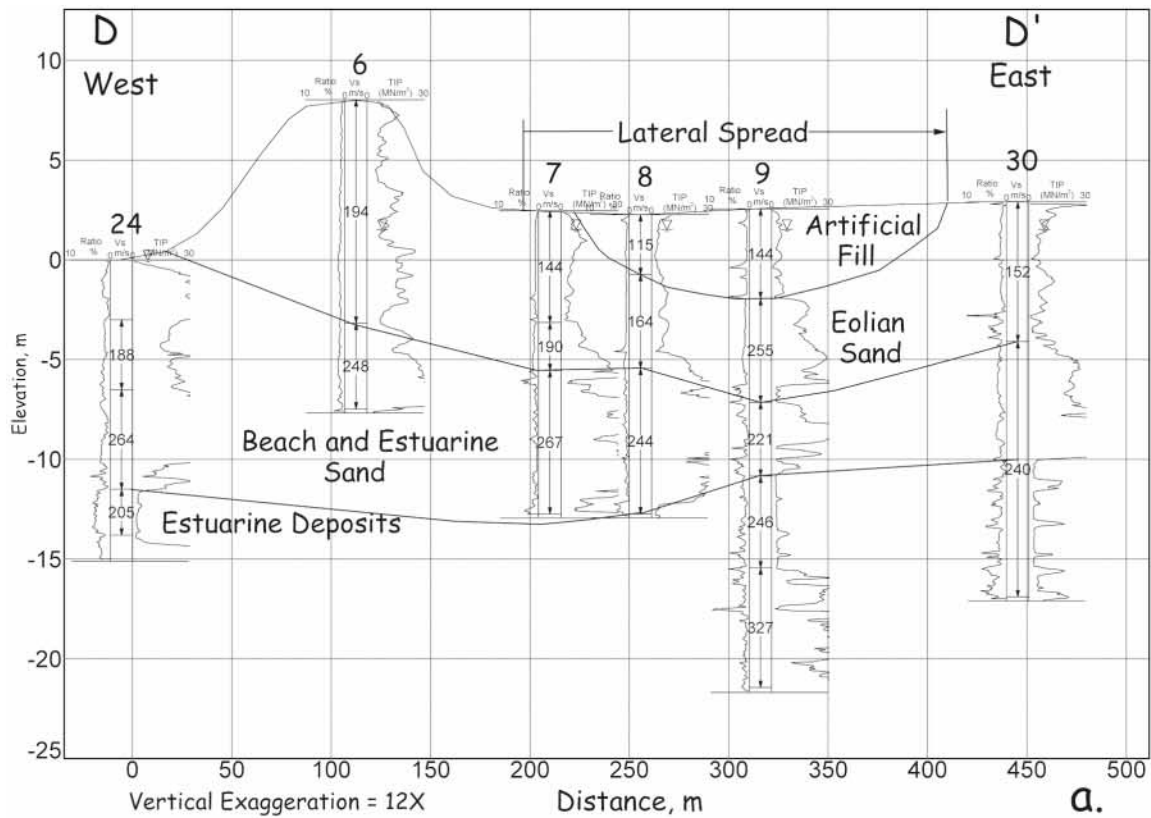
Figure 11. West–east cross section (DD') at Juanita Avenue lateral spread showing (a) geologic units and (b) factors of safety based on SCPT soundings for San Simeon earthquake (PGA = 0.25g). See Figure 2 for location. Cross section in (a) includes CPT tip resistance and friction ratio, shear-wave velocity (m/sec) of SCPT soundings, and geologic units. Water table at sounding is shown by inverted triangle.

The location of the toe of the lateral spread—the western boundary—is determined by the position of the water table. At the northern end of the spread where the toe was observed, the water table is beneath the base of the fill. The cross section across the Juanita Avenue lateral spread (Fig. 11b) also indicates that artificial fill liquefied and contributed to the lateral spreading. The conditions controlling the boundaries of the Juanita Avenue lateral spread are not as clear as they are for the Norswing Drive lateral spread. Although the toe of the spread approximately coincides with the boundary of the artificial fill, the western part of the lateral spread is underlain only by undisturbed eolian sand. Artificial fill is not present there. Because FS < 1 in the undisturbed eolian sand beneath this part of the spread, liquefaction in this deposit appears to have contributed to the lateral spreading (Fig. 11b). We also did not identify artificial fill in soundings that traversed the lateral spread at McCarthy Avenue, which is one block north of Juanita Avenue. Intervals with FS < 1 were in undisturbed eolian deposits in these soundings. Thus, the Juanita Avenue lateral spread probably was caused by liquefaction of both artificial fill and undisturbed eolian deposits.

The experience at Oceano provides an opportunity to evaluate LPI as a predictor of surface manifestations of liquefaction, which is important for the application of LPI to liquefaction hazard mapping (e.g., Holzer et al., 2002; Luna and Frost, 1998). For this application, multiple soundings are randomly conducted in a surficial geologic unit, and the cumulative percent of soundings with LPI $\geq$ 5 is used to estimate the percent of the surface area of the unit that will exhibit surface manifestations of liquefaction (Holzer et al., 2006). A cumulative frequency plot (not shown here) of LPI values computed for the 37 soundings at Oceano with a M 6.5 earthquake and PGA = 0.25g indicates 17% had LPI $\geq$ 5. This percent overestimates the area at Oceano that exhibited liquefaction effects, which should be the case because the soundings were located primarily at ground failures and not located randomly. An alternative evaluation of the threshold is to compare liquefaction areas to LPI values at SCPT soundings for the 2003 San Simeon earthquake (Fig. 12). For an individual sounding, Toprak and Holzer (2003) (Fig. 3b) indicate that the probability of liquefaction is 0.58 and 0.81, respectively, when LPI = 5 and 10. In general, liquefaction in Oceano occurred at locations where LPI $\geq$ 5. Although not rigorous, the two evaluations support the use of LPI = 5 as the threshold proposed by Iwasaki et al. (1982) and Toprak and Holzer (2003) for liquefaction prediction.

The experience at Oceano also provides an opportunity to test the multiple linear regression (MLR) procedure of Youd et al. (2002) to estimate lateral spread displacement. In this instance, an equivalent source distance, R_{eq}, must be calculated because of site amplification. For a PGA = 0.25g and an earthquake magnitude of 6.5, the R_{eq} is approximately 15 km. Using this distance in the MLR equation with a ground slope of 5%, a T_{15} (cumulative thickness of saturated

granular material with corrected blow counts less than 15) of 1.5 m, and the soil property values listed in Table 1, the predicted lateral spread displacement is 0.25 m, which is consistent with the measured displacements of less than 0.3 m.

Discussion

Mainshock ground motion at Oceano was enhanced by two processes: rupture directivity and local site amplification. In combination, they sufficiently elevated ground motion to cause liquefaction at the unexpected distance of 63 km from the rupture surface. Although it is difficult to separate precisely the contribution of each process to the ground motion at Oceano, the contributions can be estimated if the Lopez Lake PGA of 0.13g is assumed to approximate the input ground motion at Oceano. To estimate the contribution from rupture directivity, the Lopez Lake PGA can be compared with the median value estimated by Boore et al. (1997). The predicted median PGA is 0.06g for a soft rock site (V_{S30} = 620 m/sec) and 0.08g for a stiff soil site (V_{S30} = 360 m/sec). This suggests rupture directivity may have increased ground motion at Lopez Lake (and Oceano) by approximately 60–100%. The contribution from local site amplification can be estimated by comparing the inferred PGA at Oceano, 0.25g, with the PGA at Lopez Lake. The comparison suggests PGA was approximately doubled by local site amplification. If these estimates of the contributions from each process are valid, it indicates that neither rupture directivity nor local site amplification by itself would have produced a PGA level capable of causing significant liquefaction at Oceano.

Three different types of deposits liquefied at Oceano: sandy artificial fill, young eolian sand, and fluvial deposits. However, the largest and most damaging lateral spread, Norswing Drive, was caused by liquefaction of artificial fill. Factors of safety from penetration tests predict that a continuous interval at the base of the fill liquefied and was the locus of subsurface deformation in this lateral spread. In addition, the head of this lateral spread coincided with the boundary between the artificial fill and undisturbed eolian deposits. The other damaging lateral spread, Juanita Avenue, was caused by liquefaction in both artificial fill and undisturbed eolian deposits. Although the location of the toe appears to be determined by the boundary of the artificial fill, we could not identify the geologic conditions that controlled the location of the head of the lateral spread.

Two aspects of the use of LPI in the study of liquefaction at Oceano are significant. First, the use of LPI to estimate PGA suggests LPI may have application at paleoliquefaction sites for identifying potential earthquake scenarios that could have caused the liquefaction. By computing LPI values from multiple soundings at these sites for a variety of earthquake scenarios, the scenarios that do not cause LPI $\geq$ 5 could be excluded. Second, a threshold value of LPI = 5 generally
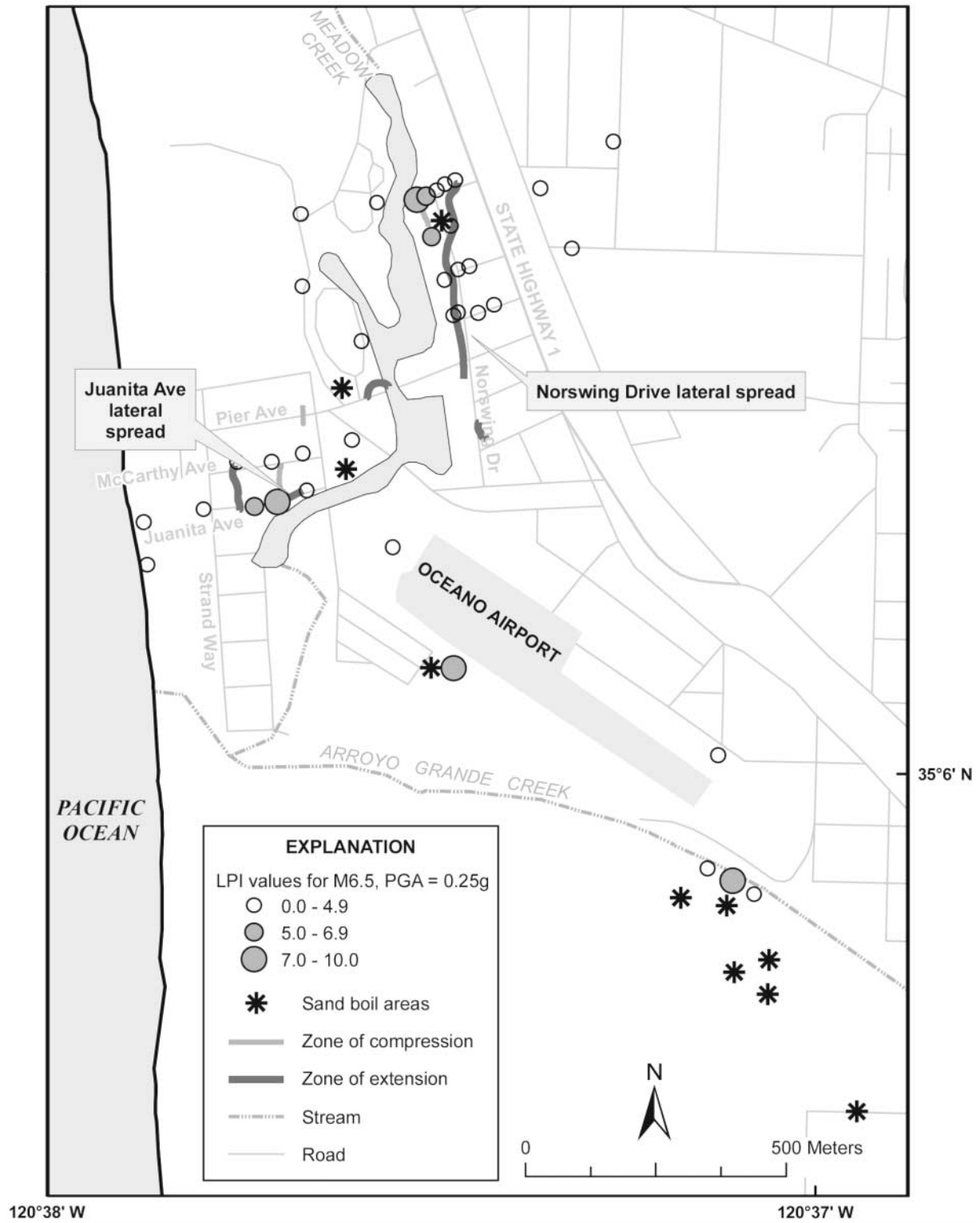
Figure 12. Map of liquefaction sites and LPI computed at SCPT soundings for the *M* 6.5 San Simeon earthquake for a PGA = 0.25*g*.

predicted the regional distribution of liquefaction at Oceano. This supports use of LPI $\geq$ 5 as the criterion for liquefaction in liquefaction hazard mapping.

The 63-km distance of Oceano from the San Simeon earthquake is a reminder of the limitations of empirical upper-bound curves that predict maximum distance to liquefaction. Distant occurrences like Oceano result from special combinations of seismological and geotechnical factors. These may include crustal path effects, rupture directivity, local amplification, and liquefaction susceptibility. Only when all of these factors are maximized is liquefaction at the maximum distance potentially realized. This realization also assumes that significant seismic energy is radiated on the rupture surface near the boundary closest to the liquefaction, a condition that may not be met.

Finally, liquefaction at Oceano is a reminder of the potential vulnerability of parts of some coastal communities to distant earthquakes. Developments on artificial fill placed over thick accumulations of unconsolidated fine-grained estuarine and marine sediment are particularly vulnerable to distant earthquakes because of their potential for local amplification of seismic shaking and high-liquefaction potential. This has been demonstrated now in two different modern earthquakes in California. The responses of the Marina District, Oakland Harbor, and Treasure Island to the Loma Prieta earthquake in 1989 (Holzer, 1998) were very similar to that of Oceano in 2003. A special combination of conditions—critical reflections off the Mohorovicic discontinuity, rupture directivity, and local site amplification—combined to increase ground shaking in 1989 to levels that liquefied susceptible artificial sandy fills at each of the Bay area sites. As a result, unusually severe damage occurred despite the 84-km distance from the Loma Prieta earthquake (Fig. 4).

Acknowledgments

References

Ambraseys, N. N. (1988). Engineering seismology, *Earthquake Eng. Struct. Dyn.* **17,** 1–105.

Boatwright, J., and L. C. Seekins (2004). Directivity in the near-field and regional recordings of the 22 December 2003 San Simeon earthquake, *Seism. Res. Lett.* **74,** 265.

Boatwright, J., L. C. Seekins, T. E. Fumal, and C. S. Mueller (1991). Ground motion amplification in the Marina District, *Bull. Seism. Soc. Am.* **81,** 1980–1997.

Boore, D. M., W. B. Joyner, and T. E. Fumal (1997). Empirical near-source attenuation relations for horizontal and vertical components of peak ground acceleration, peak ground velocity, and pseudo-absolute acceleration response spectra, *Seism. Res. Lett.* **68,** 154–179.

BSSC (2001). 2000 Edition NEHRP recommended provisions for seismic regulations for new buildings and other structures, FEMA 368, Part 1 (provisions), Federal Emergency Management Agency, Washington, D.C., 374 pp.

Di Alessandro, C., and J. Boatwright (2006). A stochastic estimate of ground motion at Oceano, California, for the M6.5 December 22, 2003, San Simeon earthquake, derived from aftershock recordings, *Bull. Seism. Soc. Am.* (in press).

Hardebeck, J. L., J. Boatwright, D. Dreger, R. Goel, V. Grazier, K. Hudnut, C. Ji, L. Jones, J. Langbein, J. Lin, E. Roeloffs, R. Simpson, K. Stark, R. Stein, and J. Tinsley (2004). Preliminary report on the 22 December 2003, M6.5 San Simeon, California, earthquake, *Seism. Res. Lett.* **75,** 155–172.

Holzer, T. L. (1998). Introduction, in *The Loma Prieta, California, Earthquake of October 17, 1989—Liquefaction*, T. L. Holzer (Editor), *U.S. Geol. Surv. Profess. Pap. 1551-B*, B1–B8.

Holzer, T. L., M. J. Bennett, T. E. Noce, A. C. Padovani, and J. C. Tinsley III (2002). Liquefaction hazard and shaking amplification maps of Alameda, Berkeley, Emeryville, Oakland, and Piedmont: A digital database, *U.S. Geol. Surv. Open-file Rept. 02-296*, http://geopubs.wr.usgs.gov/open-file/of02-296 (last accessed October 2005).

Holzer, T. L., M. J. Bennett, T. E. Noce, A. C. Padovani, and J. C. Tinsley III (2006). Liquefaction hazard mapping with LPI in the greater Oakland area, California, *Earthquake Spectra* **22** (in press).

Holzer, T. L., T. E. Noce, M. J. Bennett, C. Di Alessandro, J. Boatwright, J. C. Tinsley, III, R. W. Sell, and L. I. Rosenberg (2004). Liquefaction-induced lateral spreading at Oceano, California, during the 2003 San Simeon earthquake, *U.S. Geol. Surv. Open-file Rept. 2004-1269*, http://pubs.usgs.gov/of/2004/1269 (last accessed October 2005).

Iwasaki, T., F. Tatsuoka, K-i. Tokida, and S. Yasuda (1978). A practical method for assessing soil liquefaction potential based on case studies at various sites in Japan, in *Proc. of the 2nd International Conference on Microzonation*, San Francisco, California, 26 November–1 December 1978, 885–896.

Iwasaki, T., K-i. Tokida, F. Tatsuoka, S. Watanabe, S. Yasuda, and H. Sato (1982). Microzonation for soil liquefaction potential using simplified methods, in *Proc. of the 3rd International Conference on Earthquake Microzonation*, Seattle, Washington, 28 June–1 July 1982, 1319–1330.

Luna, R., and D. J. Frost (1998). Spatial liquefaction analysis system, *J. Comput. Civil Eng.* **12,** 48–56.

Robertson, P. K., and C. E. Wride (1997). Cyclic liquefaction and its evaluation based on the SPT and CPT, in *Evaluation of Liquefaction Resistance of Soils*, T. L. Youd and I. M. Idriss (Editors), National Center for Earthquake Engineering Research Tech. Rept. NCEER-97-0022, 41–87.

Seed, H. B., and I. M. Idriss (1971). Simplified procedure for evaluating soil liquefaction potential, *J. Soil Mech. Found. Eng. ASCE* **97,** 1249–1273.

Seed, H. B., K. Tokimatsu, L. F. Harder, and R. M. Chung (1985). Influence of SPT procedures in soil liquefaction resistance evaluations, *J. Geotech. Eng. ASCE* **111,** 1425–1445.

Toprak, S., and T. L. Holzer (2003). Liquefaction potential index: field assessment, *J. Geotech. Geoenviron. Eng. ASCE* **129,** 315–322.

Vucetic, M., and R. Dobry (1991). Effect of soil plasticity on cyclic response, *J. Geotech. Geoenviron. Eng. ASCE* **117,** 89–107.

Wald, D. A., V. Quitoriano, T. H. Heaton, and H. Kanamori (1999). Relationship between peak ground acceleration, peak ground velocity, and Modified Mercalli Intensity in California, *Earthquake Spectra* **15,** 557–564.

Weber, E. N., and F. T. Hanamura (1970). Sea-water intrusion: Pismo-Guadalupe area, California Department of Water Resources Bulletin No. 63-3, 76 pp.

Wills, C. J., M. Petersen, W. A. Bryant, M. Reichle, G. J. Saucedo, S. Tan, G. Taylor, and J. Treiman (2000). A site-conditions map for California based on geology and shear-wave velocity, *Bull. Seism. Soc. Am.* **90,** 187–208.

Youd, T. L., C. M. Hansen, and S. F. Bartlett (2002). Revised MLR equations for prediction of lateral spread displacement, *J. Geotech. Geoenviron. Eng. ASCE* **128,** 1007–1017.

Youd, T. L., I. M. Idriss, R. D. Andrus, I. Arango, G. Castro, J. T. Christian, R. Dobry, W. D. Liam Finn, L. F. Harder Jr., M. E. Hynes, K. Ishihara, J. P. Koester, S. S. C. Liao, W. F. Marcuson III, G. R. Martin, J. K. Mitchell, Y. Moriwaki, M. S. Power, P. K. Robertson, R. B. Seed, and K. H. Stokoe II (2001). Liquefaction resistance of soils: summary report from the 1996 NCEER and 1998 NCEER/NSF workshops on evaluation of liquefaction resistance of soils, *J. Geotech. Geoenviron. Eng. ASCE* **127,** 817–833.

Appendix A: Liquefaction Potential

The liquefaction potential of sediment beneath Oceano was evaluated with the factor of safety calculated with the Seed-Idriss simplified procedure (Seed and Idriss, 1971; Seed *et al.*, 1985; Youd *et al.*, 2001). The FS in the simplified procedure is the ratio of capacity of a soil element to resist liquefaction to the seismic demand imposed on it. Capacity to resist liquefaction, the cyclic resistance ratio, was computed from penetration resistance measured by cone penetration testing (Robertson and Wride, 1997). Seismic demand was computed with the cyclic stress ratio, which is proportional to PGA (Youd *et al.*, 2001).

The spatial variability of liquefaction potential in Oceano was evaluated with the LPI defined by Iwasaki *et al.* (1978). The index assumes that the severity of liquefaction is proportional to (1) the cumulative thickness of liquefied layers; (2) the proximity of liquefied layers to the surface; and (3) the amount by which the FS is less than 1.0. The index evaluates liquefaction to a depth of 20 m. The index was defined as:

$$\text{LPI} = \int_0^{20m} F \, w(z) \, dz \qquad (A1)$$

where

$$F = 1 - \text{FS} \quad \text{for FS} \leq 1$$
$$F = 0 \qquad \qquad \text{for FS} > 1$$

$w(z) = 10 - 0.5 \, z$, where z is the depth in meters.

FS was computed in the present investigation with the simplified procedure as modified for application to cone penetration testing by Robertson and Wride (1997).

Although the FS calculated from the simplified procedure is used to compute LPI, the index has two advantages. First, LPI predicts the performance of the whole soil column whereas the simplified procedure predicts the performance of a soil element. By combining all of the factors of safety from a single SCPT sounding into a single value, LPI provides a spatially distributed parameter for regional evaluations of liquefaction potential. Second, values of LPI have been empirically correlated with the severity of surface manifestations of liquefaction (Iwasaki *et al.*, 1982; Toprak and Holzer, 2003). With the simplified procedure, an additional evaluation is required to predict how a site will respond.

U.S. Geological Survey
345 Middlefield Road, MS977
Menlo Park, California 94025
  (T.L.H., T.E.N., M.J.B., J.C.T.)

San Luis Obispo County Planning and Building Department
County Government Center
1050 Monterey Street
San Luis Obispo, California 93408
  (L.I.R.)